



## PAPER

## Negative differential resistance of viscous electron flow in graphene

## OPEN ACCESS

RECEIVED  
20 May 2024REVISED  
23 September 2024ACCEPTED FOR PUBLICATION  
31 October 2024PUBLISHED  
11 November 2024

Original Content from  
this work may be used  
under the terms of the  
[Creative Commons  
Attribution 4.0 licence](#).

Any further distribution  
of this work must  
maintain attribution to  
the author(s) and the title  
of the work, journal  
citation and DOI.



Jorge Estrada-Álvarez\* , Elena Díaz and Francisco Domínguez-Adame

GISC, Departamento de Física de Materiales, Universidad Complutense, E-28040 Madrid, Spain

\* Author to whom any correspondence should be addressed.

E-mail: [adame@fis.ucm.es](mailto:adame@fis.ucm.es)**Keywords:** viscous electron flow, negative differential resistance, graphene**Abstract**

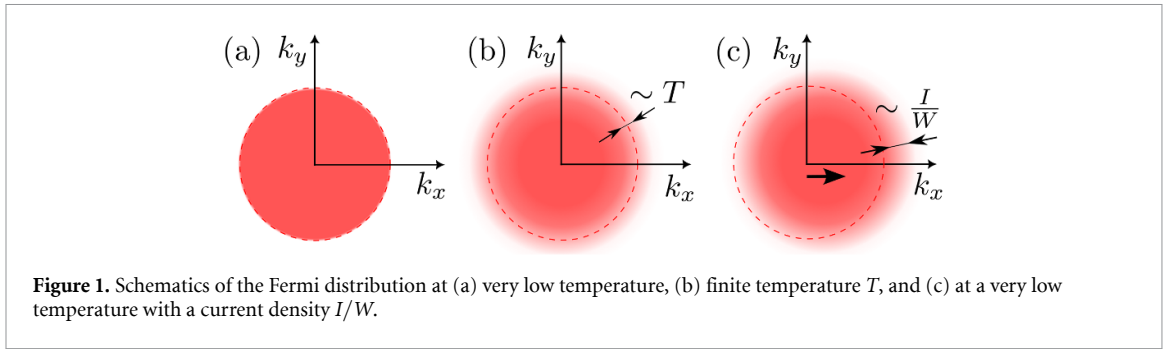
Negative differential resistance (NDR) devices show a decrease in the voltage drop with increasing current, an advantageous feature for amplifying and oscillating circuits. We introduce a NDR mechanism based on the electron hydrodynamics of two dimensional (2D) materials. An increase of the current in the system favors electron-electron collisions so that a ballistic-hydrodynamic transition takes place and the device resistance is reduced. This phenomenon results in NDR provided that the electron's mean free path is much longer than the device size. We discuss the strategies towards NDR and find that geometrically engineered devices make it possible to achieve NDR in graphene with  $\sim 200$  nm sized geometrical features. This NDR mechanism is revealed as a new hydrodynamic signature, particularly relevant in graphene devices for 2D electronics and high-frequency operation.

Two dimensional (2D) materials exhibit novel physical phenomena. This is the case of viscous electron flow, a transport regime where electrons behave like a conventional fluid [1–4]. Progress in graphene and other 2D materials has boosted the search of hydrodynamic signatures over the last few years. Some prominent signatures are the electronic Poiseuille flow [1, 5, 6] and the formation of electronic whirlpools associated with negative resistance (different from negative differential resistance) in a four-terminal device [7–10], as well as the archetypal superballistic conduction [11]. First studied by Gurzhi [12], superballistic conduction involves a collective motion of electrons which, unlike in the ballistic regime, can better adapt their path to the geometry of a device. Hence, the electrical resistance falls below the ballistic limit [13].

Collective dynamics of interacting electrons is achieved by favoring frequent electron-electron collisions. They are forbidden at zero temperature due to the Pauli blockade (see figure 1(a)), but bringing electrons out of their ground state makes them possible. There are two main approaches to be followed to achieve this goal. First, the temperature of the device  $T$  can be increased (see figure 1(b)). This phenomenon gives rise to the already mentioned

superballistic conduction or Gurzhi effect [11, 12]. Second, the electric current can be increased (see figure 1(c)). This affects the electronic temperature  $T_e$  independently of the lattice temperature  $T$ . The increase of the current accounts for an electronic temperature rise and thus, for a decrease in the device resistance as well. The latter can be referred to as the Molenkamp effect after its discoverer in (Al,Ga)As heterostructures [14, 15]. The same effect was recently studied in graphene field effect transistors [7, 16]. Here, the magnitude of interest is the differential resistance  $R_d = dV/dI$ , where  $V$  is the voltage drop and  $I$  is the current across the device. Experiments show, for some range of currents, a decrease in  $R_d$  with increasing current, an effect that is stronger in graphene devices [16]. So far, however, the experimental evidence only reveals positive differential resistance  $R_d > 0$ . To the best of our knowledge, whether negative differential resistance (NDR)  $R_d < 0$  is possible is a question that has not been addressed.

Nonetheless, non-ohmic charge transport has been crucial for the development of modern electronic technology. As such, NDR is an essential property for the design of electronic circuits [17], including amplifiers and oscillators. Here, it is closely



related to the THz gap [18], for which other mechanisms such as the Dyakonov–Shur instability have been suggested [19]. Regarding the intensity-voltage characteristics, we separately consider the voltage-controlled and the current-controlled NDR. On the one hand, voltage-controlled NDR exhibits a distinctive N-shaped profile, showing a decrease in the current with increasing voltage over a given range. Voltage-controlled NDR [20, 21] appears in tunnel diodes [22, 23]. The modulation of the gate potential has been put forward to explain voltage-controlled NDR in graphene field effect transistors [24–26]. On the other hand, current-controlled NDR exhibits S-shaped characteristics, where the voltage drop decreases with increasing current for a certain current range. IMPATT diodes [27] show current-controlled NDR. There exist other mechanisms based on material instabilities [17] or the self-heating of the device, with no electronic origin which may present issues for high-frequency operation. Particularly, the absence of a gap in graphene jeopardizes the ability to build a graphene-based switch and its usage in electronic applications [28, 29]. However, the novel features of 2D electronic devices and their unique response at high-frequency fields make it desirable to find alternative NDR mechanisms in graphene.

In this work, we demonstrate that a 2D viscous electron fluid can exhibit current-controlled NDR, when the ballistic-hydrodynamic transition is driven by an increase of the electric current. We find that the NDR performance is dramatically improved when the sample geometry is properly engineered. We last explore the properties of this NDR mechanism for several electronic functionalities.

Our description for electronic flow starts from the semiclassical Boltzmann transport equation (BTE) [30–33]. By considering perturbations around the equilibrium Fermi distribution, it reads

$$\hat{\mathbf{k}} \cdot \nabla_{\mathbf{r}} \left( g - \frac{eV}{mv_F} \right) + \frac{\partial_{\theta} g}{l_B} + \frac{g}{l_e} + \frac{g - g^{ee}}{l_{ee}} = 0, \quad (1)$$

where  $g(\mathbf{r}, \theta)$  is a distribution accounting for the excess of electrons moving in the direction  $\hat{\mathbf{k}}(\theta) = \mathbf{k}/k = (\cos\theta, \sin\theta)$  with momentum  $\mathbf{k}$  at position

$\mathbf{r}$  (see [34] for details). We assume an isotropic material with a Fermi velocity  $v_F = \hbar k_F/m$ , where  $k_F$  is the Fermi momentum and  $m$  is the cyclotron mass [35]. The electrons, with charge  $-e$ , are subjected to an electric potential  $V = V(\mathbf{r})$  and a perpendicular magnetic field  $\mathbf{B}$ , which introduces the cyclotron radius  $l_B = mv_F/eB$ . Last, under Callaway’s approximation [4, 15, 36], electron scattering introduces two different mean free paths. First,  $l_e$  accounts for the inelastic collisions against impurities and phonons, which do not conserve momentum. Second,  $l_{ee}$  accounts for the elastic electron-electron collisions, which conserve momentum. As a consequence, the distribution relaxes to a distribution  $g^{ee}(\mathbf{r}, \theta) \simeq u_x(\mathbf{r}) \cos\theta + u_y(\mathbf{r}) \sin\theta$  that moves with the electron’s drift velocity  $\mathbf{u}(\mathbf{r}) = (u_x(\mathbf{r}), u_y(\mathbf{r})) = (1/\pi) \int_0^{2\pi} \hat{\mathbf{k}}(\theta) g(\mathbf{r}, \theta) d\theta$ .

Non-linear effects [37] in an electron fluid are mainly due to the change in  $l_{ee}$  with increasing current [7, 15, 16]. We also comment on NDR beyond Callaway’s approximation, in the tomographic regimes, where more relaxation times are taken into account [38].

To proceed, we assume that the non-equilibrium distribution function is a smooth function of the polar angle  $\theta$  and expand  $g(\mathbf{r}, \theta)$  up to second order harmonics [31]. We obtain the continuity equation and the equivalent equation to the Navier–Stokes equation (NSE) used in conventional fluids [34]

$$\nabla_{\mathbf{r}} \cdot \mathbf{u} = 0, \quad (2a)$$

$$\begin{aligned} \nu \nabla_{\mathbf{r}}^2 \mathbf{u} - \left( \frac{eB}{m} + \nu_H \nabla_{\mathbf{r}}^2 \right) \mathbf{u} \times \hat{\mathbf{z}} - \frac{v_F}{l_e} \mathbf{u} \\ = -\frac{e}{m} \nabla_{\mathbf{r}} V, \end{aligned} \quad (2b)$$

The viscosity and the Hall viscosity are given as

$$\nu = \frac{v_F (l_e^{-1} + l_{ee}^{-1})}{4 (l_e^{-1} + l_{ee}^{-1})^2 + 16 l_B^{-2}}, \quad (3a)$$

$$\nu_H = \frac{v_F l_B^{-1}}{2 (l_e^{-1} + l_{ee}^{-1})^2 + 8 l_B^{-2}}. \quad (3b)$$

These expressions involve non-conserving momentum scattering through the mean free

path  $l_e$  [11, 33, 39]. Notice that non-conserving momentum scattering also reveals itself as a dissipative term in the NSE (2b). We use the following expression for the electron-electron mean free path [11, 40]

$$\frac{1}{l_{ee}} = \frac{\pi k_F}{4} \left( \frac{T_e}{T_F} \right)^2 \ln \left( \frac{2T_F}{T_e} \right), \quad (4)$$

where  $T_e$  is the temperature of the electron fluid [15] and  $T_F = \hbar^2 k_F^2 / 2mk_B$  is the Fermi temperature. This expression is valid for a Fermi liquid ( $T_e \ll T_F$ ). The electron temperature  $T_e$ , which results from the lattice temperature  $T$  and the electron kinematics under a current  $I$ , may be estimated as

$$T_e^2 \approx T^2 + \frac{4}{\mathcal{N}} \frac{\pi \hbar^2}{e^2 k_B^2} \frac{I^2}{nW^2}, \quad (5)$$

where  $n$  is the electron density,  $\mathcal{N} = 4$  is the number of equivalent spins and valleys in graphene, and  $W$  is the width of the device. The definition of a temperature describing local dynamics [41], and a distribution like the one schematically shown in figure 1(c), was guaranteed by frequent electron-electron collisions  $l_{ee} \ll W$ . In fact, this is the case in the hydrodynamic regime where we seek NDR. To derive the equation, the drift velocity of the electrons  $v_d = j/ne$ , which is proportional to the current density  $j$ , is used to determine the momentum shift in the Fermi distribution  $\delta k = k_F v_d / v_F$ . The broadening of the distribution in terms of energy is, therefore,  $k_B T_e^l = \delta \varepsilon = \hbar v_F \delta k$ . In a general scenario, both the lattice temperature  $T$  and the current-driven electron temperature  $T_e^l$  contribute to the final electron  $T_e$ . Thus, we obtain equation (5) by considering both contributions in quadrature as usually done with the widths of two distributions. Notice that it is common to assume a global temperature  $T_e$  for the whole sample. Global thermalization lies upon the hypothesis of very infrequent inelastic scattering events  $l_e \rightarrow \infty$ . However, in this work, we go beyond this approximation and also study hydrodynamic models where  $T_e$  is locally defined with the local current density instead of  $I/W$ . In addition, notice that the second term in  $T_e$  may slightly be corrected by a geometrical factor that could be analyzed with current-noise measurements [42]. In any case, it is the dependence of the second term on  $I^2$  that enables the emergence of NDR. Therefore, the same basic strategies to find NDR can be considered, regardless of the particular expression of such term. Last, notice that the increase in the electron temperature is primarily due to the applied current, that brings the electrons out of its equilibrium distribution, a physical mechanism distinct from Joule dissipation.

Viscous flow is affected by the scattering of the electrons at the sample edges, so we consider two representative boundary conditions [43] that supplement equations (2). First, we study a diffusive (DF)

edge, where electrons are scattered at the edges in all directions, resulting in a partial slip condition with the slip length  $\xi = 3\pi 4\nu/v_F$ . Second, a partially specular (PS) edge with  $\xi = (8/d - 16/3\pi)\nu/v_F$ , for the dispersion coefficient  $d \equiv \sqrt{\pi} \hbar^2 l_c k_F^3 \lesssim 1$ , where  $h$  is the edge roughness and  $l_c$  is its correlation length (see [34, 43]).

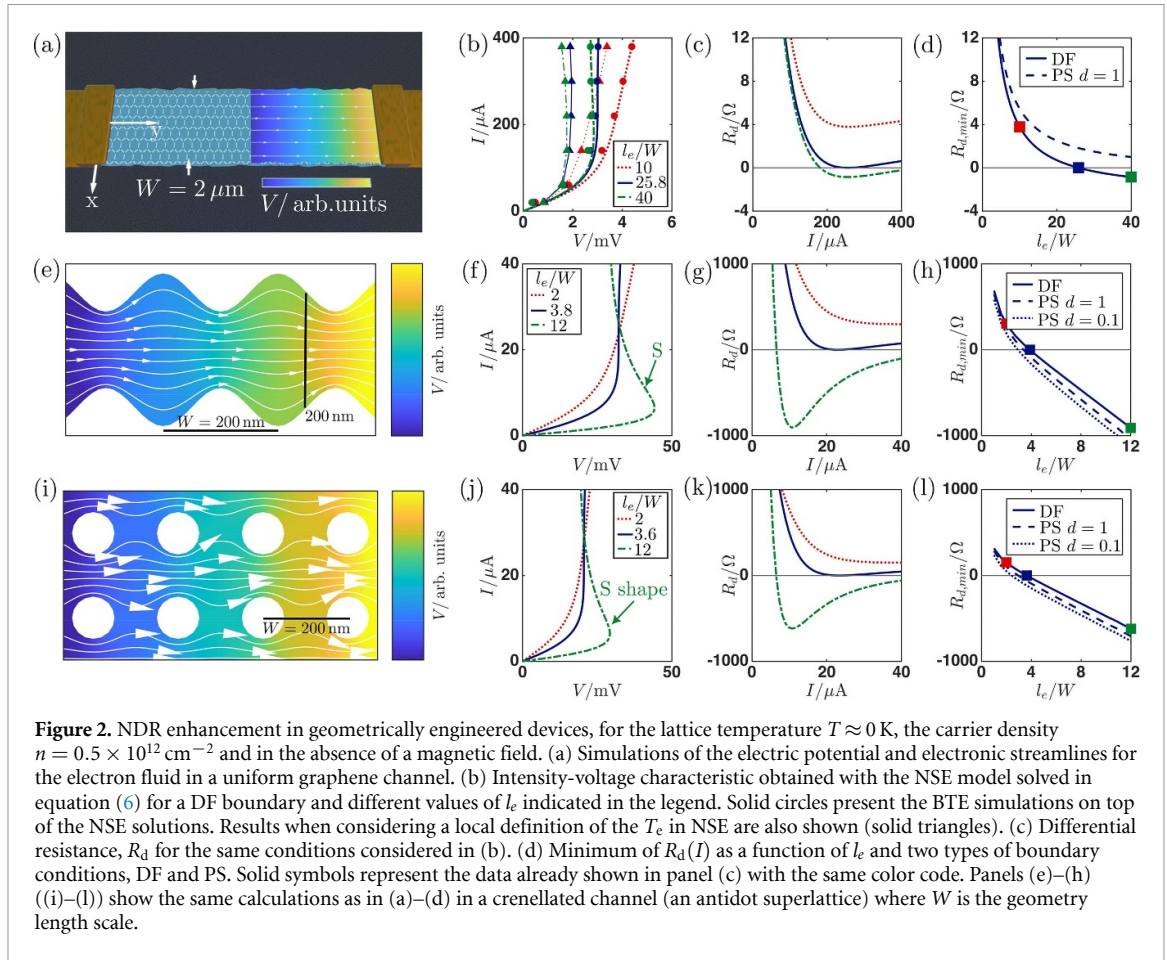
The NSE can be solved to find the velocity  $\mathbf{u}(r)$  and the potential  $V(r)$ , which can be used to determine the current density  $\mathbf{j} = -en\mathbf{u}$ , whose integral across the device is the current  $I$ . The ratio between the voltage drop at the two ends of the sample and the current gives the electrical resistance. Particularly the NSE has a close solution for a very long channel of width  $W$  and length  $L$ , and the resistance is found to be

$$R = \frac{mv_FL}{e^2 n l_e W} \left( 1 - \frac{2D_\nu/W}{\coth(W/2D_\nu) + \xi/D_\nu} \right)^{-1}, \quad (6)$$

where  $D_\nu \equiv \sqrt{\nu l_e / v_F}$ . In arbitrary geometries the NSE is solved with a conforming Galerkin finite element method with Taylor–Hood elements for geometry triangulation [44], taking sizes  $h < 0.2W$  to ensure convergence. The current is set at the contacts, which are at least 2 periods away from the region studied to compute the resistance and solve the linear system resulting from the finite element method. Last, we use a Runge–Kutta 4 method to find the electron streamlines, and numerical integration for the total current (see [34]). When a local definition of temperature is considered, we use an iterative approach based on consecutive solutions for  $\mathbf{u}(r)$  to compute  $l_{ee}$  until convergence is achieved. On the other hand, in order to obtain the electrical current by the BTE formalism we first find the  $g(r, \theta)$  distribution, which is integrated to find  $\mathbf{u}$ . We numerically solved the BTE in a uniform channel using a conforming Galerkin finite element method [45] on Matlab, writing the solution as  $g(x, \theta) = \sum_{n=1}^N \sum_{m=1}^M \phi_n(x) \varphi_m(\theta)$  with  $M = 40$  tent elements and the product of two consecutive elements for the spatial part and  $M = 32$  tent functions for the angular part.

Figures 2(a)–(d) show the results of the simulations of the voltage-intensity characteristics in a uniform channel of width  $W = 2 \mu\text{m}$ . Panels (b) and (c) display the intensity-voltage characteristic and the corresponding differential resistance  $R_d = dV/dI$  for several values of the mean free path  $l_e$ . All simulations account for a carrier density  $n = 0.5 \times 10^{12} \text{ cm}^{-2}$ . We chose this value to favor  $l_e \gg W$  [7], which is one of the conditions we demonstrate for NDR. Although NDR would arise at lower  $I$  near the charge neutrality point, we rather avoid the issues related to thermal activation and charge inhomogeneities.

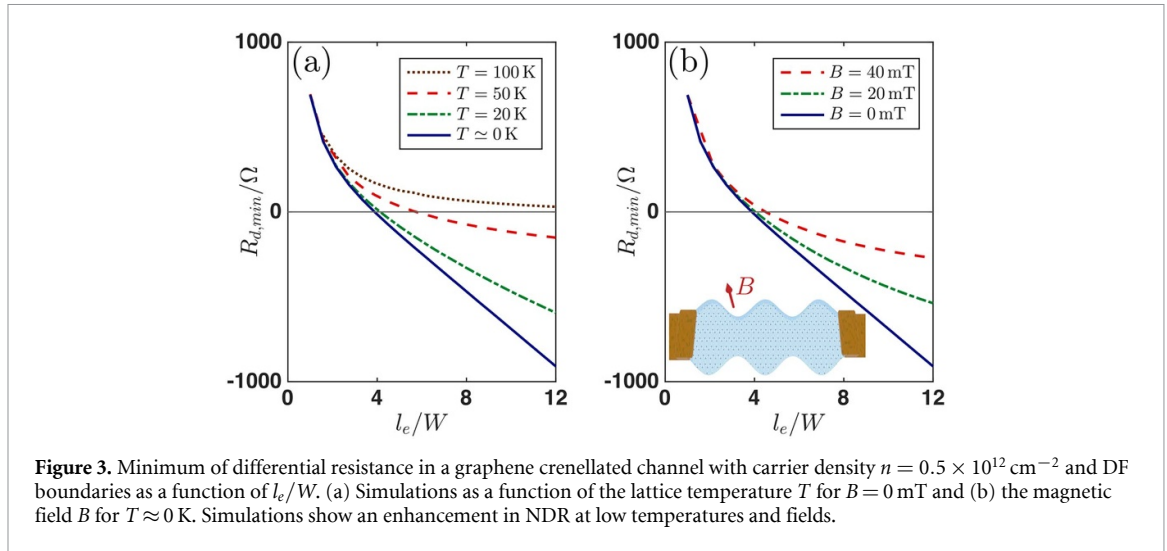
In these panels, we consider  $T \approx 0 \text{ K}$  and DF edges in the absence of a magnetic field. We show the



predictions of the NSE model (solid lines) which result in equation (6) and the BTE results (circles). Both descriptions predict NDR, and their results nearly overlap for higher currents, where NDR occurs. As demonstrated in equations (4) and (5),  $l_{ee}$  is smaller due to an increase in  $I$  and the hydrodynamic description becomes valid [7, 11, 16] (see also [34] for a discussion of the transport regimes). Regarding the tomographic dynamics [38], when elastic collisions have two relaxation rates, our results are robust even when the relaxation rate of the odd parity modes,  $l_{ee}^o$ , is much larger than that of the even parity modes,  $l_{ee}^e$ ,  $l_{ee}^o = 10l_{ee}^e$ . Consequently, we will use the NSE hydrodynamic model to study NDR hereafter in complex geometries (figures 2(e)–(l)). In addition, figure 2(b) shows (triangles) the NSE predictions using a local electron temperature where  $I/W$  is replaced by the local current density for comparison. This is a dramatically different approach that neglects the transfer of the thermal fluctuations within the whole sample. Despite the slight quantitative deviation, we prove that NDR still occurs under the surmise of a local temperature. As a conclusion, the assumption of a global temperature  $T_e$  is not crucial for the emergence of NDR. Indeed, if the length of the channel is much larger than its width, as considered here, the variation of the temperature profiles is negligible [42]. As shown in figure 2, we find S-type NDR in the setups studied

in this work. As aforementioned, increasing the current reduces the value of  $l_{ee}$ , and this decrease produces the transition from the ballistic regime to viscous electron flow. The resulting collective behavior, eventually, reduces the resistance. This is consistent with the fact that there are two possible values of the current  $I$  for the same potential drop. However, only the highest one (leading to a reduction of  $l_{ee}$ ) drives fully collective electron dynamics.

Figure 2(d) shows that NDR only appears above a critical value of  $l_e \gtrsim 25.8W$ . Indeed, the decay of  $R = V/I$  within the ballistic-hydrodynamic transition needs to be very fast to achieve NDR. Conduction at a large enough current becomes diffusive and the resistance reaches an asymptotic value that scales as  $\sim l_e^{-1}$ . Hence, a larger change in the resistance within the transition is expected for clean samples which enables NDR. Furthermore, systems with PS boundaries (dashed line in figure 2(d)) only exhibit NDR for even larger values of  $l_e$ , which agrees with the fact that the hydrodynamic transition shifts to higher  $l_e$  in systems with PS boundaries [34]. In a uniform channel, only the lateral edges may bend the electron flow, so very specular boundaries result in a uniform electron flow, not affected by elastic collisions. In summary, the  $l_e$  values required for NDR in a uniform channel are not easily achievable. In addition to the lack of robustness regarding the edge scattering



properties, we conclude that our theory is consistent with previous experimental evidence where NDR was not observed [7, 15, 16].

In view of such difficulties, new strategies need to be considered. Further bending the electron flow seems to be a reasonable strategy, so we suggest geometrically engineering the sample. Consequently, we study the crenellated channel [39] shown in figure 2(e), where  $W = 200 \text{ nm}$  is a length scale, which matches both the mean width and the oscillation's period. We also study an antidot superlattice [46] as a feasible proposal in figure 2(i), where  $W = 200 \text{ nm}$  is the distance between the centers of two adjacent holes. Notice that in all cases  $W$  gives an estimate of the average distance within collisions with boundaries. The resistance  $R_d$  and the current  $I$  that we show in figure 2 are normalized to one period of every geometry. Both the crenellated channel and the antidot superlattice improve the results by an order of magnitude. Now NDR appears at  $l_e \gtrsim 3.8 W$  or  $l_e \gtrsim 3.6 W$  respectively, meaning  $l_e \sim 1 \mu\text{m}$ , a realistic inelastic mean free path in graphene [7]. Current values of  $I \sim 20 \mu\text{A}$  are also reasonable considering that  $I = 300 \mu\text{A}$  was reached in [7, 16]. Most importantly, the phenomenon barely depends on the boundary condition. In particular, it is slightly enhanced for PS with low  $d$ . Notice that unlike in the uniform channel, the electron fluid can more easily follow the geometrical features when this edge condition applies. This corresponds to smooth edges such as those obtained with cryo-etching [47]. The enhancement of the NDR effect when geometrically engineering the sample agrees with the fact that the Gurzhi effect [12] is not usually measured in uniform channels but in constrictions [11].

Now, let us analyze the role of the lattice temperature  $T$ . Figure 3(a) extends figure 2(h) in the crenellated channel for several values of  $T$ , demonstrating that the NDR effect reduces with increasing  $T$ . As aforementioned, there must be a large decrease in

$R = V/I$  within the ballistic-hydrodynamic transition for NDR to arise. However, transport at low currents at finite temperature  $T$  can already support superballistic conduction with low resistance [11]. Hence, the global decay from such a reduced value is not quick enough when varying the applied current to produce NDR. Furthermore, we need  $T_e \ll T_F$  for equation (4) to be valid. If the temperature  $T_e$  is increased, such dependency approximately transforms to  $l_{ee} \propto 1/T_e$  [11], which is not quick enough, and NDR disappears. In this regard, notice that lattice heating must be avoided by a proper design that favors heat dissipation. Although this effect seems quite cumbersome in GaAs experiments [15], it is not that serious in graphene samples [16]. Indeed, some measurements, even at very low density of carriers, do not show an appreciable Joule heating up to  $300 \mu\text{A}$ . Another side effect regarding the temperature  $T$  is the increase of the electron-phonon scattering and the reduction of  $l_e$ . However, for low temperatures  $\lesssim 50 \text{ K}$ , the dispersion relation of graphene does not show a significant increase in phonon scattering. If a steady lattice temperature  $T$  can be expected regardless of high-frequency electronic oscillations, the role of this heating can be considered in an effective  $l_e$  value.

Last, let us explore the dependence with the magnetic field in figure 3(b). Similar to the effect of  $T$ , the magnetic field keeps us apart from the ballistic regime [34] even at low currents, and opposes the quick descent in  $R = V/I$  that would otherwise enable NDR. Notice that our current proposal of studying the effects of the magnetic field spans the traditional scope of the experiments on the Molenkamp effect [16]. Moreover, it provides additional evidence of the hydrodynamic nature of the NDR mechanism.

Now that we have studied NDR, let us comment on three device proposals. Voltage regulators displaying S-type characteristics are the most immediate application. In this devices  $dV/dI \approx 0$ ,

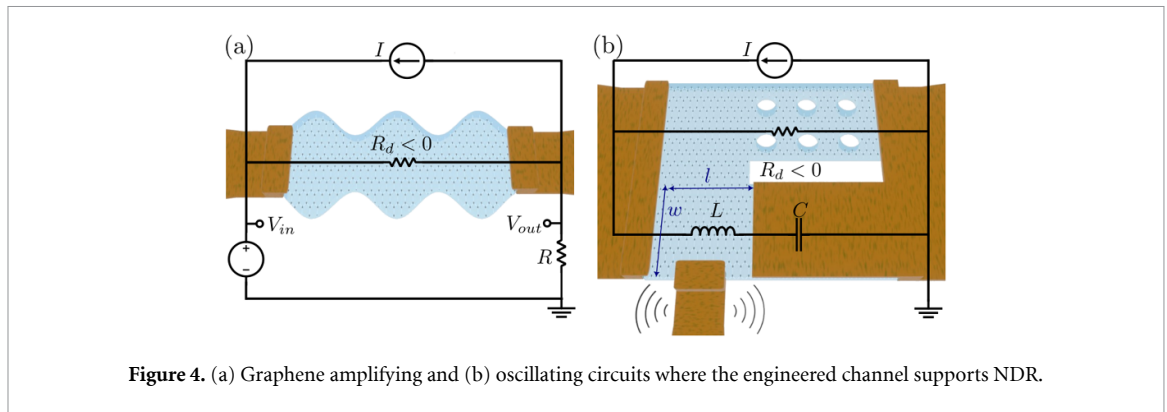


Figure 4. (a) Graphene amplifying and (b) oscillating circuits where the engineered channel supports NDR.

keeping a constant voltage when varying the electric current, as we found for the critical case when  $l_e = 11.7 \text{ W}$  (see figures 2(b), (f) and (j)). Notice that regulators do not need  $dV/dI < 0$  strictly.

Moreover, a NDR device with a current source can also be used as an amplifier, as shown in figure 4(a). Here external signals increase their amplitude provided that the resistance of the circuit is smaller than  $-R_d$ . This is not a serious concern since several devices could be connected in series to achieve it. Remarkably, there is not a threshold voltage for this mechanism to operate. Finally, a NDR device with a capacitor  $C$  and an inductor  $L$  acts as an oscillator. Indeed if it is pumped with an external source, under the same condition of  $-R_d$  larger than the resistance of the circuit, it generates oscillations of frequency  $\omega \approx (LC)^{-1/2}$  aimed at producing electromagnetic radiation. We can achieve this condition by reducing the length  $l$  of the capacitor and the inductor. Figure 4(b) depicts a sample architecture on a graphene flake, with a capacitance  $C \approx 2e^2 \sqrt{\pi} l w / (\hbar v_F \sqrt{\pi})$  mainly due to quantum effects [48] and an inductance [49]  $L \approx ml / (e^2 n w)$  due to the carriers inertia. A straightforward calculation yields  $\omega \approx v_F / (\sqrt{2} l)$  which is 0.1 THz for  $l \approx 1 \mu\text{m}$ . For NDR to persist,  $v_F / \omega \ll W$  or equivalently  $l \ll W$  should be fulfilled. Moreover in order to increase the operating frequency one mainly has to reduce the size of the geometrical features. Thus, this NDR mechanism may overcome some of the difficulties of other oscillating mechanisms, such as the Dyakonov–Shur instability [19, 50] and continue the efforts to close the THz gap [18].

In this work, we prove that the 2D viscous electron flow in graphene exhibits NDR if the transition from ballistic to hydrodynamic transport is triggered by an increase in the current, which gives rise to a decrease in the electron-electron mean free path. This phenomenon reveals itself as a novel hydrodynamic signature. The main strategies towards NDR are to geometrically engineer the device and to ensure that the ratio between the sample geometrical features and the inelastic mean free path  $W/l_e$  remains small. In conclusion, this NDR mechanism enables electronic

applications in 2D materials such as graphene and could be used in high-frequency devices as an alternative to the Dyakonov–Shur instability. The broad interest in viscous electron fluids and the prospect of novel applications opens a challenging search for electronic devices displaying lower differential resistance.

### Data availability statement

All data that support the findings of this study are included within the article (and any supplementary files).

### Acknowledgments

We thank R Brito, R Soto, E Diez, M Amado, and J Bernabeu for valuable discussions. This work was supported by the Spanish Ministry of Science and Innovation (Grant PID2022-136285NB-C31). We also acknowledge the support from the “(MAD2D-CM)-UCM” project funded by Comunidad de Madrid, by the Recovery, Transformation and Resilience Plan, and by NextGenerationEU from the European Union. J E-A acknowledges support from the Ministerio de Ciencia, Innovación y Universidades (Grant FPU22/01039).

### ORCID iDs

Jorge Estrada-Álvarez  <https://orcid.org/0000-0001-8036-7168>

Elena Díaz  <https://orcid.org/0000-0002-2324-5946>

Francisco Domínguez-Adame  <https://orcid.org/0000-0002-5256-4196>

### References

- [1] Sulpizio J A et al 2019 *Nature* **576** 75
- [2] Polini M and Geim A K 2020 *Phys. Today* **73** 28
- [3] Narozhny B N 2022 *Riv. Nuovo Cimento* **45** 1
- [4] Varnavides G, Yacoby A, Felser C and Narang P 2023 *Nat. Rev. Mater.* **8** 726
- [5] Jenkins A, Baumann S, Zhou H, Meynell S A, Daipeng Y, Watanabe K, Taniguchi T, Lucas A, Young A F and Jayich A C B 2022 *Phys. Rev. Lett.* **129** 087701

- [6] Glazov M 2021 *2D Mater.* **9** 015027
- [7] Bandurin D A et al 2016 *Science* **351** 1055
- [8] Bandurin D A, Shytov A V, Levitov L S, Kumar R K, Berdyugin A I, Shalom M B, Grigorieva I V, Geim A K and Falkovich G 2018 *Nat. Commun.* **9** 4533
- [9] Aharon-Steinberg A et al 2022 *Nature* **607** 74
- [10] Danz S and Narozhny B N 2020 *2D Mater.* **7** 035001
- [11] Kumar R K et al 2017 *Nat. Phys.* **13** 1182
- [12] Gurzhi R N 1963 *J. Exp. Theor. Phys.* **17** 521
- [13] Huang W, Paul T, Perrin M and Calame M 2024 *2D Mater.* **11** 033001
- [14] Molenkamp L W and De Jong M J M 1994 *Solid State Electron.* **37** 551
- [15] De Jong M J M and Molenkamp L W 1995 *Phys. Rev. B* **51** 13389
- [16] Huang W, Paul T, Watanabe K, Taniguchi T, Perrin M L and Calame M 2023 *Phys. Rev. Res.* **5** 023075
- [17] Dragoman M and Dragoman D 2022 *Solid State Electron.* **197** 108464
- [18] Leitenstorfer A et al 2023 *J. Phys. D: Appl. Phys.* **56** 223001
- [19] Dyakonov M and Shur M 1993 *Phys. Rev. Lett.* **71** 2465
- [20] Gunn J B 1963 *Solid State Commun.* **1** 88
- [21] Poole C and Darwazeh I 2016 *Microwave Active Circuit Analysis and Design* (Academic)
- [22] Esaki L 1958 *Phys. Rev.* **109** 603
- [23] Esaki L 1974 *Science* **183** 1149
- [24] Sharma P, Bernard L S, Bazigos A, Magrez A and Ionescu A M 2015 *ACS Nano* **9** 620
- [25] Song Y, Liu Y, Feng X, Yan F and Zhang W 2018 *Phys. Chem. Chem. Phys.* **20** 1560
- [26] Song Y, Wu H-C and Guo Y 2013 *Appl. Phys. Lett.* **102** 093118
- [27] Read Jr. W T 1958 *Bell Syst. Tech. J.* **37** 401
- [28] Katsnelson M I, Novoselov K S and Geim A K 2006 *Nat. Phys.* **2** 620
- [29] Young A F and Kim P 2009 *Nat. Phys.* **5** 222
- [30] Di Ventra M 2008 *Electrical Transport in Nanoscale Systems* (Cambridge University Press)
- [31] Holder T, Queiroz R, Scaffidi T, Silberstein N, Rozen A, Sulpizio J A, Ella L, Ilani S and Stern A 2019 *Phys. Rev. B* **100** 245305
- [32] Kapralov K and Svintsov D 2022 *Phys. Rev. B* **106** 115415
- [33] Guo H, Ilseven E, Falkovich G and Levitov L S 2017 *Proc. Natl Acad. Sci. USA* **114** 3068
- [34] Estrada-Álvarez J, Dominguez-Adame F and Díaz E 2024 *Commun. Phys.* **7** 138
- [35] Neto A C, Guinea F, Peres N M, Novoselov K S and Geim A K 2009 *Rev. Mod. Phys.* **81** 109
- [36] Callaway J 1959 *Phys. Rev.* **113** 1046
- [37] Hui A, Oganesyan V and Kim E-A 2021 *Phys. Rev. B* **103** 235152
- [38] Ledwith P, Guo H, Shytov A and Levitov L 2019 *Phys. Rev. Lett.* **123** 116601
- [39] Keser A et al 2021 *Phys. Rev. X* **11** 031030
- [40] Giuliani G and Vignale G 2008 *Quantum Theory of the Electron Liquid* (Cambridge University Press)
- [41] Soto R 2016 *Kinetic Theory and Transport Phenomena* vol 25 (Oxford University Press)
- [42] Hui A and Skinner B 2023 *Phys. Rev. Lett.* **130** 256301
- [43] Kiselev E I and Schmalian J 2019 *Phys. Rev. B* **99** 035430
- [44] Engwirda D and Ivers D 2016 *Comput. Aided Des.* **72** 157
- [45] Ciarlet P G 2002 *The Finite Element Method for Elliptic Problems* (SIAM)
- [46] Estrada-Álvarez J et al 2024 Superballistic conduction in hydrodynamic antidot graphene superlattices (arXiv:2407.04527)
- [47] Clericò V, Delgado-Notario J A, Saiz-Bretín M, Malyshev A V, Meziani Y M, Hidalgo P, Méndez B, Amado M, Domínguez-Adame F and Diez E 2019 *Sci. Rep.* **9** 1
- [48] Xia J, Chen F, Li J and Tao N 2009 *Nat. Nanotechnol.* **4** 505
- [49] Kang J et al 2018 *Nat. Electron.* **1** 46
- [50] Crabb J, Cantos-Roman X, Jornet J M and Aizin G R 2021 *Phys. Rev. B* **104** 155440